

Geology

Topographic modulation of fault kinematics in the Himalaya and Tibet

--Manuscript Draft--

Manuscript Number:	G39391
Full Title:	Topographic modulation of fault kinematics in the Himalaya and Tibet
Short Title:	Topographic modulation of fault kinematics in the Himalaya and Tibet
Article Type:	Article
Keywords:	faults; topography; Tibet; stress; Gorkha
Corresponding Author:	Richard Styron Earth Analysis Pavia, Lombardy ITALY
Corresponding Author Secondary Information:	
Corresponding Author's Institution:	Earth Analysis
Corresponding Author's Secondary Institution:	
First Author:	Richard Styron
First Author Secondary Information:	
Order of Authors:	Richard Styron
Order of Authors Secondary Information:	
Manuscript Region of Origin:	NEPAL
Abstract:	Throughout the Himalaya and Tibet, moderate- to high-elevation strike-slip faults undergo extensional stepovers where they cross pre-existing higher topography. Related seismological data have long been explained by an influential orogen-scale cross-section model where high-elevation normal faulting and low-elevation thrust faulting result from laterally-invariant horizontal tectonic stress and vertical stress that varies with topography; however, this model cannot incorporate strike-slip faulting or ~10 km wavelength topography. Therefore I introduce a 3D elastic model describing the modulation of fault kinematics by shorter-wavelength topographic stress, and show how this may tightly constrain the tectonic stress field. I then calculate the topographic stress field on the Western Nepal Fault System, and use topographic stresses and observed fault kinematics to invert for the tectonic stress field. The results yield a maximum tectonic compression of 0-0.2 pgz and minimum tectonic compression of -0.1-0.1 pgz, and reproduce kinematics from normal, strike-slip and thrust faults and earthquakes in and around western Nepal, including the 2015 Gorkha earthquake. This demonstrates that where vertical and a horizontal principal stress are near equal, 1-10 km scale variations in topography can change fault kinematics, and that pre-existing topography can influence the location of subsequent faults and stepovers.
Suggested Reviewers:	Eric Cowgill University of California Davis escowgill@ucdavis.edu knowledgeable about Tibetan active tectonics and fault-stress interactions
	Whitney Behr University of Texas at Austin behr@utexas.edu Very knowledgeable about active faulting and stress
	John Townend Victoria University of Wellington john.townend@vuw.ac.nz Expert on stress inversions and faulting

1 Topographic modulation of fault kinematics in the
2 Himalaya and Tibet

3 **Richard H. Styron¹**

4 *¹Earth Analysis, Via Luigi Porta 10, Pavia, Italy 27100*

5 **ABSTRACT**

6 Throughout the Himalaya and Tibet, moderate- to high-elevation strike-slip faults
7 undergo extensional stepovers where they cross pre-existing higher topography. Related
8 seismological data have long been explained by an influential orogen-scale cross-section
9 model where high-elevation normal faulting and low-elevation thrust faulting result from
10 laterally-invariant horizontal tectonic stress and vertical stress that varies with
11 topography; however, this model cannot incorporate strike-slip faulting or ~10 km
12 wavelength topography. Therefore I introduce a 3D elastic model describing the
13 modulation of fault kinematics by shorter-wavelength topographic stress, and show how
14 this may tightly constrain the tectonic stress field. I then calculate the topographic stress
15 field on the Western Nepal Fault System, and use topographic stresses and observed fault
16 kinematics to invert for the tectonic stress field. The results yield a maximum tectonic
17 compression of 0–0.2 $\rho g z$ and minimum tectonic compression of -0.1–0.1 $\rho g z$, and
18 reproduce kinematics from normal, strike-slip and thrust faults and earthquakes in and
19 around western Nepal, including the 2015 Gorkha earthquake. This demonstrates that
20 where vertical and a horizontal principal stress are near equal, 1-10 km scale variations in
21 topography can change fault kinematics, and that pre-existing topography can influence
22 the location of subsequent faults and stepovers.

23 **Introduction**

24 In the Himalaya and Tibet, it has long been observed that thrust earthquakes take
25 place at the low-elevation rangefronts surrounding the plateau, while normal and strike-
26 slip earthquakes occur in the elevated interior (e.g., *Molnar and Tapponnier, 1978; Elliott*
27 *et al., 2010*) (Figure 1a). *Molnar and Lyon-Caen (1988)* offered an influential physical
28 explanation for this simultaneous low-elevation reverse faulting and high-elevation
29 normal faulting: Horizontal tectonic compression σ_H (integrated over the crustal column)
30 is essentially spatially invariant, while vertical compression σ_V at depth varies with the
31 height of the overlying terrain. At low elevations, $\sigma_H > \sigma_V$, leading to crustal thickening,
32 while at higher elevations, $\sigma_V > \sigma_H$, causing crustal extension.

33 These observations and hypotheses concern entire orogens. Whether they apply at
34 smaller scales is a natural question, though unaddressed. The analytical model by *Molnar*
35 *and Lyon-Caen (1988)* rests on the assumption of isostatically-supported topography,
36 which is valid over 10^2 – 10^3 km scales (i.e., orogens), but may not be over 1-10 km
37 (mountain to mountain range) scales, where topography is mostly supported elastically
38 (e.g., *Bollinger et al. 2004*). Additionally, topographic slopes at these scales may impart
39 locally substantial stresses in the upper crust, which may be smoothed out at larger scales.
40 The motivating observations are typically earthquake focal mechanisms, which are too
41 sparse spatially and from too short a time window to fully describe high-resolution
42 deformation.

43 However, neotectonic mapping provides a more complete description of the
44 deformation field integrated over longer timescales (10^3 - 10^5 years) and offers better
45 spatial coverage and resolution as well. Recent neotectonic maps of the Himalaya and

46 Tibet reveal a rich interaction between fault type and elevation over 1-100 km scales
47 (Figure 1). These observations document changes in the kinematics of large fault systems
48 where the faults cross smaller topographic features (ridges to mountain ranges); as the
49 topography is often known to be older than the active faults, it is likely that topography
50 modifies fault kinematics at these scales as well, though the mechanisms may be different
51 than in the orogen-scale, isostatic case. Documenting this phenomenon is the first
52 objective of this study.

53 If topography is capable of modifying fault kinematics, then the total (tectonic
54 plus topographic) stress field must resolve on the faults with shear stress directions that
55 are consistent with the directions of fault slip. Therefore, if the topographic stresses can
56 be calculated, these stresses and the fault kinematics may be used to constrain the
57 tectonic stress field. Precise estimation of tectonic stress is a major advancement for
58 understanding earth processes. Stress is generally unknown at the order of magnitude
59 level, despite being a fundamental physical property of the earth, and the primary control
60 on the earth's deformation. Accurate stress estimates are critical for understanding the
61 distribution of seismicity in time and space, as well as the physical properties and
62 evolution of faults and orogens. This quantification is the second objective of this study.

63 **Fault kinematic transitions and topography in Tibet and the Himalaya**

64 Many fault zones within the Tibetan plateau and vicinity show transitions in fault
65 kinematics with changes in topography (Figure 1). These are best displayed in
66 transtensional fault zones in the elevated interior of the plateau, consistent with the
67 hypothesis that Tibet is at the maximum elevation that can be sustained by horizontal
68 tectonic compression (e.g., *Molnar and Lyon-Caen, 1988*). For example, the sinistral

69 Longmu Co–Gozha Co fault system has a major extensional stepover where the fault
70 crosses the western Kunlun Shan, where the 2008 M_w 7.1 Yutian earthquake occurred
71 (*Xu et al., 2013*). Left-lateral faulting continues to the northeast of the high mountains as
72 the faults merge with the Altyn Tagh Fault. Similarly, the transtensional Yibug Caka and
73 Mugu Purou rifts in central Tibet show local extensional stepovers where topography is
74 elevated (*Taylor et al., 2003; Ratschbacher et al., 2011*), and the conjugate strike-slip
75 systems to their south link to rifts where regional elevation steps higher. This is evident in
76 individual earthquakes as well: *Chang et al. (2016)* observe localized extensional fault
77 scarps near isolated high mountains on the western end of the 2001 M_w 7.8 Kunlun
78 rupture.

79 Additionally, most isolated topographic highs on the plateau outside of
80 transtensional zones are cut by active normal faults that do not extend far into the lower
81 surroundings; the Gangdese (Figure 1b) and Tanggula Ranges (Figure 1a) are prime
82 examples. In these locations, the horizontal differential stress may not be great enough
83 for fault failure, but high σ_V underneath the ranges causes localized normal faulting.

84 Perhaps the most clear example of topographic modulation of fault kinematics is
85 on the southeastern Karakoram–Western Nepal Fault System, which undergoes three
86 distinct extensional stepovers, one for each instance in which the fault system intersects
87 pre-existing topographic highs (Figure 1b).

88 The Karakoram Fault (KF) is a major dextral fault on the boundary between the
89 northwestern Himalaya and southwestern Tibet. The KF is purely strike-slip through
90 most of its length but has a transtensional zone where it cuts through the Gangdese Range

91 called the Gar Basin (*Sanchez et al., 2010*), and terminates at the Pulan Graben
92 (dominated by the Gurla Mandhata Detachment, GMD) where the KF hits the northern
93 Himalaya (*Murphy et al., 2002*). Some or all of the KF slip is transferred to the GMD and
94 south into the Himalaya along the Humla Fault (*Murphy and Burgess, 2006*).

95 Though the nature of fault connectivity remains unclear, it is likely that dextral
96 slip continues through the Himalayan wedge along the Western Nepal Fault System
97 (WNFS). Dextral and normal slip has been observed on the Tibrikot and Dogari segments
98 of the WNFS (*Murphy et al., 2014; Silver et al., 2015*). Additional dextral fault offsets
99 have been observed on the Talphi and Bari Gad Faults to the northwest and southeast of
100 the Tibrikot fault (*Nakata, 1989*).

101 A striking feature of the overall geometry of the KF-GMD-WNFS faults is that
102 extensional stepovers occur wherever the strike-slip faults encounter locally high terrain
103 (Figure 1b). The higher terrain in all cases predates the strike-slip faulting along the KF-
104 WNFS system: The Gangdese Range was a regional topographic high and sediment
105 source by the Oligocene (*Leary et al., 2016*), predating the post-middle Miocene faulting
106 in Gar Basin (*Sanchez et al., 2010*), while the Himalaya was uplifted to near modern
107 elevation by the Miocene (*Garzione et al., 2000*), before extension. Extension along the
108 GMD has resulted in great uplift of the footwall (>7700 m), but normal faulting must
109 cause a net decrease in regional elevation despite local footwall uplift. Additionally,
110 faults associated with the current dextral-normal slip regime cut north-dipping brittle and
111 ductile fault fabrics associated with the uplift of the Himalaya (*Silver et al., 2015*). It may
112 be that the WNFS becomes transpressive in its low-elevation southern extent, as the Bari

113 Gad fault nears the active Himalayan frontal folds and thrusts; this is observed on the
114 symmetrical Altyn Tagh fault system on Tibet's northern margin (*Cowgill et al., 2004*).

115 **Three-dimensional topographic and tectonic stresses**

116 The regional-scale topography and stress relationship described here share the
117 central concept developed in the orogen-scale models, that changes in fault style result
118 from variable, primarily vertical topographic stresses superposed on relatively invariant,
119 primarily horizontal tectonic stresses (Figure 2). However, the regional model has some
120 key differences, as well.

121 First, this problem is inherently three-dimensional. Faults of all kinematic types in
122 the Himalaya and Tibet accommodate ~N-S shortening, ~E-W extension, or both (Figure
123 1). This allows us to expand the model's dimensionality: Whereas the two-dimensional
124 model has $\sigma_H > \sigma_V$ (reverse faulting) in the of moderate elevations, and $\sigma_H > \sigma_h > \sigma_V$ in
125 the highlands, where σ_h is the minimum principal horizontal stress (Figure 2). This
126 expansion enables us to consider faults of all styles and orientations (not only those
127 striking perpendicularly to the 2D model's cross-section), and to calculate the full 3D
128 stress tensor field. Futhermore, if σ_H and σ_h are not near equal, there may be a large
129 elevation gap between reverse and normal faulting, leading to large uncertainties in stress
130 estimations in the 2D model (*Richardson and Coblenz, 1994*). By considering all three
131 fault styles and principal stresses, the uncertainties are much reduced.

132 Secondly, shorter-wavelength topography is supported elastically rather than
133 isostatically (e.g., *Bollinger et al., 2004*). This means that topographic stresses may vary
134 dramatically over short horizontal and vertical distances, slopes may impart locally strong
135 horizontal stress, and the perturbation to the stress field produced by topography extends

136 outward and downward rather than simply being a simply vertical sum of the weight of
137 the overlying rocks. As a result, short-wavelength topographic stresses may be spatially
138 variable and resolve very differently along-strike and down-dip on a through-going fault.

139 Finally, the regional model does not require invariance of tectonic stress over
140 $10^2 - 10^3$ km, only over $10^0 - 10^2$ km. Tectonic stress may change over longer
141 distances due to changes in boundary conditions (e.g., plate driving forces) and
142 lithospheric rheology. While *Molnar and Lyon-Caen (1988)* do provide compelling
143 arguments for stress invariance across orogens, such invariance is not a requirement of
144 this model. Consistent application of stress inversions using the regional model (as
145 below) in many locations throughout an orogen may serve as a test of orogen-scale
146 tectonic stress invariance.

147 **Topographic stress**

148 To test the hypothesis that the topography-fault kinematics relationship is based
149 on a varying topographic stress superposed on a laterally-invariant tectonic stress field, I
150 seek to reproduce the observed fault kinematics by calculating the topographic and
151 tectonic stress fields, and resolving them on 3D fault models in the region, following
152 methods outlined in *Styron and Hetland (2015)*. The topographic stress calculations are
153 deterministic, as topography is well known and allowable variation in the Earth's elastic
154 moduli does not meaningfully modify the results. The tectonic stresses are solved for
155 using a Bayesian inversion scheme. To avoid overfitting and assess the veracity of results
156 beyond the study region, the inversion is performed on two relatively well-studied faults,
157 the Gurla Mandhata and Tibrikot-Dogari faults, and then validated on additional
158 deformation data in the region: a coseismic slip model from the 2015 M_w 7.8 Gorkha,

159 Nepal earthquake (*Galetzka et al., 2015*) and pre-Gorkha focal mechanisms throughout
160 the region. The two faults modeled here were selected because the fault geometry and
161 kinematics are well known through field (*Murphy et al., 2002; Silver et al., 2015*) and
162 thermochronological (*McCallister et al., 2014*) studies; the other faults in the WNFS have
163 not received sufficient study to model confidently.

164 The topographic stresses are calculated through elastic halfspace methods
165 following *Liu and Zoback (1992)* and *Styron and Hetland (2015)*, by a convolution of
166 functions describing the distribution of topographic loading on the halfspace surface with
167 Green's functions describing the propagation of stresses in the halfspace from vertical and
168 horizontal point loads on the surface. This results in a 3D array with the 3x3 topographic
169 stress tensor calculated at every point (500 m horizontal resolution, 1 km vertical
170 resolution) in a ~840x700 km region. The halfspace surface is set to sea level, though
171 calculations above 1500 m below sea level are discarded due to concerns of
172 overestimating shallow topographic stress where slopes are steep, a known limitation of
173 the perturbation-expansion method used.

174 The Gurla Mandhata and Tibrikot-Dogari fault traces are extended to depth based
175 on constraints from structural data and thermal modeling. The fault surfaces are made into
176 a triangular mesh, and the stress tensors are then interpolated onto them using barycentric
177 interpolation. The rake of the maximum shear stress on each fault patch is calculated
178 based on the strike and dip of that fault patch.

179 **Tectonic stress**

180 I then solve for the allowable tectonic stresses through a Bayesian inversion,
181 seeking to minimize the misfit between the rake of the resolved total stress tensor

182 (topographic plus tectonic) and the observed slip rake. The tectonic stress field T is
183 assumed to increase linearly with depth below the halfspace surface (*Townend and*
184 *Zoback, 2000*), and so is scaled to be a fraction of lithostatic pressure below the halfspace
185 surface (i.e., $\rho g z$, where $\rho = 2700 \text{ kg m}^{-3}$). T is horizontal, and has three components:
186 T_{\max} , T_{\min} and T_{az} (the azimuth of T_{\max}). T_{\max} has a uniform prior from [0—1] $\rho g z$,
187 T_{\min} has a uniform prior of [-1—1] T_{\max} (T_{\min} is by definition smaller than T_{\max} and
188 therefore cannot be independently defined in terms of $\rho g z$), and T_{az} has a uniform prior
189 of 0° — 359° . Each sample of T is then rotated to T_{N-S} , T_{E-W} , and T_{N-E} (the horizontal
190 shear stress) and added to the topographic stress tensor at each point.

191 For each of 1 million samples, the mean rake misfit $\overline{\lambda^m}$ is calculated as the mean
192 of the absolute value of the rake differences between the observed slip rake and modeled
193 maximum shear stress rake. Then, the relative likelihood of each sample set is calculated
194 as $p(D|T) = \frac{\exp(\kappa \cos \overline{\lambda^m})}{\exp(\kappa \cos \overline{\lambda_{\max}^m})}$ where κ is a scale term, reflecting the uncertainty in the rake
195 data.

196 The posteriors $p(T|D)$ are then sampled proportionally to the relative likelihood,
197 following Bayes' rule: $p(T|D) \propto p(T) p(D|T)$.

198 Results

199 Topographic stresses tend to be in the direction of fault slip, particularly for the
200 dip-slip faults, including the Gorkha rupture plane, which is loaded in a thrust sense by
201 slope-induced subhorizontal compression. Tectonic stresses are not working against
202 topography in the Himalaya.

203 The results of the tectonic stress inversion are shown in Figure 3. The maximum
204 posterior values for the joint posterior distribution (i.e., the location of the highest
205 posterior probability density in the 3-variable space) are $T_{\max} = 0.1 \rho g z$, ($\sim 2.7 \text{ MPa km}^{-1}$
206 depth), $T_{\min} = -0.1 \rho g z$, and $T_{az} = 20^\circ$. The mean absolute misfit between the observed
207 and modeled fault rakes for the maximum posterior model is 26° . The 1D marginals are
208 somewhat similar; T_{\max} has a mode at $< 0.05 \rho g z$, T_{\min} has a mode near 0, with a tensile
209 skew, and T_{az} has a mode at 20° , parallel to the direction of the Indo-Asian convergence
210 (e.g., Gan *et al.*, 2007).

211 These results agree well with regional earthquake data not used in the inversion:
212 The maximum-likelihood tectonic stresses were scaled to depth and added to the
213 topographic stress tensor at each point in a coseismic slip model from the 2015 Gorkha,
214 Nepal earthquake (Galetzka *et al.*, 2015) and pre-Gorkha focal mechanisms from the
215 central Himalaya and southern Tibet (ISC). The total stress tensors were resolved on each
216 fault plane and the predicted shear stress rake was compared to the observed slip rake.
217 The rakes matched very well ($< 30^\circ$ misfit) for nearly all data points, regardless of
218 whether the data were from thrust, normal or strike-slip earthquakes (Figure S1). This
219 confirms the predictive power of this simple model where spatially-varying topographic
220 stress coupled with depth-scaled tectonic stress control a complicated deformation field.

221 To test the effects of topographic stress (versus simply fault geometry) on
222 replicating the shear stresses on the faults, the stress inversion procedure was repeated
223 without topographic stresses on the fault planes, while holding all else constant. The
224 results yield a most-likely model with $T_{\max} = 0.05 \rho g z$, $T_{\min} = -1.15 \rho g z$, and $T_{az} =$
225 18° ; $\overline{\lambda^m}$ is about 10° higher. The strong tension for T_{\min} is required to induce normal-

226 sense shear on the extensional stepovers in the absence of strong vertical compression
227 underneath topography. Though the misfit is acceptable, it is unclear how orogen-parallel
228 tension greater than $\rho g z$ could be generated in the Himalaya; block divergence due to
229 variably-oblique convergence along the curved Himalayan front should induce some
230 tension (*McCaffrey and Nábelek, 1998*), although $\rho g z$ is quite high. Additionally, unlike
231 topographic stress, tectonic stress alone does not predict the location of extensional
232 stepovers; it simply is able to match the slip rake on the existing stepovers to some
233 degree.

234 The stress results are consistent with Himalayan thrusting: $T_{\max} = 0.1 * \rho g z \approx 7$
235 MPa on a 10° dipping plane at 15 km, which is approximately equal to the location and
236 magnitude of the maximum stress drop (~8 MPa) of the Gorkha earthquake (*Galetzka et*
237 *al., 2015*), suggesting that tectonic stress drop may have been locally complete during
238 this earthquake. However, shear stresses from topography on the Gorkha fault plane are
239 >20 MPa here, so total shear stress drop was not complete.

240 **Discussion**

241 In Tibet and the Himalaya, topography likely modulates fault kinematics over ~10
242 km scales by locally changing the relative magnitudes of σ_V to σ_H and σ_h . Pre-existing
243 topographic highs produce high σ_V in the crust beneath, causing extensional stepovers in
244 younger strike-slip faults cutting through the topography. This phenomenon is only
245 possible where the larger-scale balance of stresses is such that $\sigma_V > \sigma_H$ under
246 topographic highs but $\sigma_H > \sigma_V$ in adjacent lower locations. By computing topographic
247 stress, the orientations and magnitudes of σ_H and σ_h can be tightly constrained.

248 In the study areas, the topographic relief (not necessarily the modern elevation)
249 predates the current tectonic regime and associated faults, and is therefore capable of
250 controlling the location of releasing bends in strike-slip faults, as well as isolated grabens
251 (e.g., in the Gangdese range). This may be common in orogens with a polyphase or
252 protracted history (yielding enough paleorelief) which finally reach a broad equivalence
253 between σ_V and σ_H . However, evidence of this process may be erased with erosion, and
254 the process may even reverse as stepover-produced topography builds: *Cowgill et al.*
255 (2004) suggest that the kinematics of some stepovers on the Altyn Tagh fault change due
256 to increasing topography and σ_V .

257 The tectonic stresses estimated are, perhaps, low for creating the world's current
258 highest mountain range. They are significantly lower than those estimated at $T_{\max} =$
259 $0.5 - 1 \rho g z$ in eastern Tibet with the same methods (*Styron and Hetland, 2015*), or
260 $T_{\max} = 1.0 \rho g z$ measured from the upper 2.5 km of the SAFOD pilot hole on the San
261 Andreas (*Hickman and Zoback, 1994*). However, as differential stress is limited by the
262 strength of faults, low T_{\max} may be due to a weak Main Himalayan thrust, marking a
263 similarity with subduction zone megathrusts (e.g., *Houston, 2015*).

264 ACKNOWLEDGEMENTS

265 I thank Lydia Staisch, Kurt Sundell and Mike Taylor for comments on drafts of this
266 manuscript. All data and code can be found at https://github.com/cossatot/wnfs_stress/.

267 REFERENCES CITED

268 Bollinger, L., Avouac, J. P., Cattin, R., & Pandey, M. R. (2004). Stress buildup in the
269 Himalaya. *Journal of Geophysical Research: Solid Earth*, 109(B11).

- 270 Chang, H., Li, L. Y., Molnar, P., & Niemi, N. A. (2016). Activation of a Minor Graben
271 and Pull-Apart Basin Just East of Bukadaban during the 2001 Kunlun Earthquake
272 (Mw 7.8). *Bulletin of the Seismological Society of America*.
- 273 Elliott, J. R., Walters, R. J., England, P. C., Jackson, J. A., Li, Z., & Parsons, B. (2010).
274 Extension on the Tibetan plateau: recent normal faulting measured by InSAR and
275 body wave seismology. *Geophysical Journal International*, 183(2), 503-535.
- 276 Galetzka, J., Melgar, D., Genrich, J.F., Geng, J., Owen, S., Lindsey, E.O., Xu, X., Bock,
277 Y., Avouac, J.P., Adhikari, L.B. and Upreti, B.N., 2015. Slip pulse and resonance
278 of the Kathmandu basin during the 2015 Gorkha earthquake, Nepal. *Science*,
279 349(6252), pp.1091-1095.
- 280 Garzione, C.N., Dettman, D.L., Quade, J., DeCelles, P.G. and Butler, R.F., 2000. High
281 times on the Tibetan Plateau: Paleoelevation of the Thakkola graben, Nepal.
282 *Geology*, 28(4), pp.339-342.
- 283 Houston, H. (2015). Low friction and fault weakening revealed by rising sensitivity of
284 tremor to tidal stress. *Nature Geoscience*, 8(5), 409.
- 285 International Seismological Centre, On-line Bulletin, <http://www.isc.ac.uk>, Internatl.
286 Seismol. Cent., Thatcham, United Kingdom, 2013.
- 287 Leary, R., Orme, D.A., Laskowski, A.K., DeCelles, P.G., Kapp, P., Carrapa, B. and
288 Dettinger, M., 2016. Along-strike diachroneity in deposition of the Kailas
289 Formation in central southern Tibet: Implications for Indian slab dynamics.
290 *Geosphere*, 12(4), pp.1198-1223.

- 291 Liu, L. and Zoback, M.D., 1992. The Effect of Topography on the State of Stress in the
292 Crust: Application to the Site of the Cajon Pass Scientific Drilling Project. *Journal*
293 *of Geophysical Research*, 97(B4), pp.5095-5108.
- 294 McCaffrey, R. and Nabelek, J., 1998. Role of oblique convergence in the active
295 deformation of the Himalayas and southern Tibet plateau. *Geology*, 26(8),
296 pp.691-694.
- 297 McCallister, A.T., Taylor, M.H., Murphy, M.A., Styron, R.H. and Stockli, D.F., 2014.
298 Thermochronologic constraints on the late Cenozoic exhumation history of the
299 Gurla Mandhata metamorphic core complex, Southwestern Tibet. *Tectonics*,
300 33(2), pp.27-52.
- 301 Molnar, P. and Lyon-Caen, H., 1988. Some simple physical aspects of the support,
302 structure, and evolution of mountain belts. *Geological Society of America Special*
303 *Papers*, 218, pp.179-208.
- 304 Molnar, P. and Tapponnier, P., 1979. Active tectonics of Tibet. *Journal of Geophysical*
305 *Research: Solid Earth*, 83(B11), pp.5361-5375.
- 306 Murphy, M.A. and Burgess, W.P., 2006. Geometry, kinematics, and landscape
307 characteristics of an active transtension zone, Karakoram fault system, southwest
308 Tibet. *Journal of Structural Geology*, 28(2), pp.268-283.
- 309 Murphy, M.A., Taylor, M.H., Gosse, J., Silver, C.R.P., Whipp, D.M. and Beaumont, C.,
310 2014. Limit of strain partitioning in the Himalaya marked by large earthquakes in
311 western Nepal. *Nature Geoscience*, 7(1), pp.38-42.
- 312 Murphy, M.A., Yin, A., Kapp, P., Harrison, T.M., Manning, C.E., Ryerson, F.J., Lin, D.
313 and Jinghui, G., 2002. Structural evolution of the Gurla Mandhata detachment

- 314 system, southwest Tibet: Implications for the eastward extent of the Karakoram
315 fault system. Geological Society of America Bulletin, 114(4), pp.428-447.
- 316 Nakata, T., 1989. Active faults of the Himalaya of India and Nepal. Geological Society of
317 America Special Papers, 232, pp.243-264.
- 318 Richardson, R.M. and Coblenz, D.D., 1994. Stress modeling in the Andes: Constraints
319 on the South American intraplate stress magnitudes. Journal of Geophysical
320 Research: Solid Earth, 99(B11), pp.22015-22025.
- 321 Sanchez, V.I., Murphy, M.A., Dupré, W.R., Ding, L. and Zhang, R., 2010. Structural
322 evolution of the Neogene Gar Basin, western Tibet: Implications for releasing
323 bend development and drainage patterns. Geological Society of America Bulletin,
324 122(5-6), pp.926-945.
- 325 Silver, C.R., Murphy, M.A., Taylor, M.H., Gosse, J. and Baltz, T., 2015. Neotectonics of
326 the Western Nepal Fault System: Implications for Himalayan strain partitioning.
327 Tectonics, 34(12), pp.2494-2513.
- 328 Styron, R.H. and Hetland, E.A., 2015. The weight of the mountains: Constraints on
329 tectonic stress, friction, and fluid pressure in the 2008 Wenchuan earthquake from
330 estimates of topographic loading. Journal of Geophysical Research: Solid Earth,
331 120(4), pp.2697-2716.
- 332 Styron, R., Taylor, M. and Okoronkwo, K., 2010. Database of active structures from the
333 Indo-Asian collision. Eos, Transactions American Geophysical Union, 91(20),
334 pp.181-182.
- 335 Taylor, M., Yin, A., Ryerson, F.J., Kapp, P. and Ding, L., 2003. Conjugate strike-slip
336 faulting along the Bangong-Nujiang suture zone accommodates coeval east-west

337 extension and north-south shortening in the interior of the Tibetan Plateau.
338 Tectonics, 22(4).

339 Townend, J. and Zoback, M.D., 2000. How faulting keeps the crust strong. Geology,
340 28(5), pp.399-402.

341

342 **FIGURE CAPTIONS**

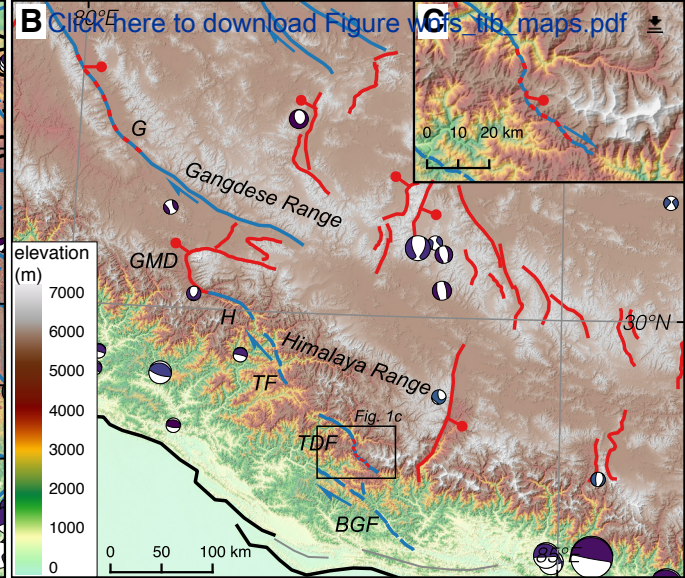
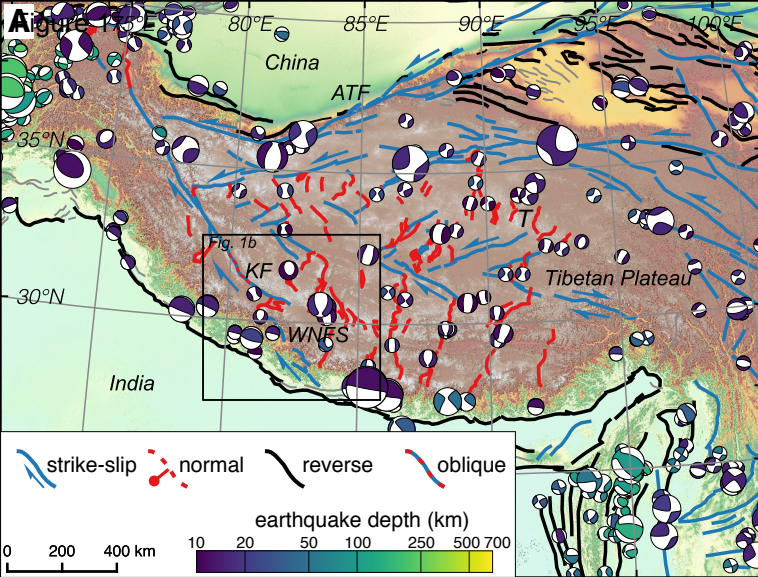
343 Figure 1A: Active faults, seismicity and topography of the Tibetan Plateau. B:
344 Map of the southeastern KF and WNFS. KF=Karakoram Fault. ATF=Altyn Tagh Fault.
345 T=Tanggula Range. GM=Gurla Mandhata Detachment. G=Gar Basin. TF=Alphali Fault.
346 TDF=Tibrikot-Dogari Faults. BGF=Bari Gad Fault. Focal mechanisms from the GCMT
347 Catalog (Ekström et al. 2012). Faults modified from HimaTibetMap v. 1.2 (Styron et al.
348 2010).

349

350 Figure 2: Schematic block diagram demonstrating the relationships between
351 stress, topography and faulting. σ_H and σ_h (represented by σ_E and σ_N) are invariant
352 across the region though σ_V varies with topography, changing fault kinematics.

353

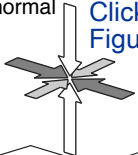
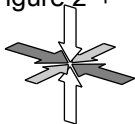
354 Figure 3A: Scatterplot with marginal histograms of the inversion results for T_{\max}
355 and T_{\min} . B: Rose diagram for T_{az} .



strike slip

normal

thrust



Click here to download
Figure block_diagram.pdf

